Supporting Information

Direct Operando Spectroscopic Observation of Oxygen Vacancies in Working Ceria-Based Gas Sensors

Ann-Kathrin Elger, Julian Baranyai, Kathrin Hofmann, Christian Hess*

Eduard-Zintl-Institut für Anorganische und Physikalische Chemie, Technische Universität Darmstadt, Alarich-Weiss-Str. 8, 64287 Darmstadt, Germany

*hess@pc.chemie.tu-darmstadt.de

Table of Contents

1. Supplementary Materials and Methods

1.1 Synthesis and Characterization

The ceria support was synthesized by decomposition of $Ce(NO_3)_3$ (Alfa Aesar, 99.5%) at 600°C for 12 h using a heating rate of 6°C/min. A second calcination using the same protocol was applied after the sample had cooled to room temperature. Using N_2 adsorption and applying the Brunauer–Emmett–Teller (BET) model, the specific surface area of the ceria sample was determined as 57 m^2/g. Transmission electron microscopy (TEM) characterization (JEOL JEM-2100F, 200 kV) revealed the presence of 10–15 nm sized crystals with a $CeO_2(111)$ surface termination as well as stepped sites. Please refer to Ref. [1] for details of the synthesis and TEM characterization. X-ray powder diffraction (XRD, STOE, STADIP, $Cu_{K\alpha1}$-radiation, λ = 1.54060 Å, Ge[111] monochromator) revealed a cubic, fluorite-type structure (see Figure S-1).

Gold was deposited onto the support by means of deposition precipitation, i.e., CeO_2 was first suspended in deionized water and the pH value was adjusted to 9 using a 0.1 M NaOH solution. Then a 10^{-3} M solution of $HAuCl_4 \cdot 3H_2O$ (Sigma Aldrich, 99.999%) was adjusted to pH 9; an appropriate amount of the solution was added to the ceria suspension to obtain a nominal fraction of 0.5 wt% (1 wt%) gold on ceria. Then, the suspension was heated to 65°C for at least 2 h and cooled down to room temperature during treatment in a sonicator (~30 min). The product was centrifuged, washed with 12% ammonia solution and water three times, and dried at 85°C for 48 h. Finally, samples were calcined at 500°C for 4 h. Using N_2 adsorption and applying the Brunauer–Emmett–Teller (BET) model, the specific surface area of the Au/ceria samples was determined to be 61 m^2/g and 62 m^2/g for 0.5 wt% Au/CeO_2 and 1 wt% Au/CeO_2, respectively. As described in Ref. [1] in more detail, gold particles in 0.5 wt% Au/CeO_2 were characterized in scanning TEM (STEM) mode, enabling ^{58}Ce and ^{79}Au to be distinguished. STEM and TEM images show a small number of gold particles with a size of 10 nm. Consistent with this observation is that XRD analysis reveals only a cubic, fluorite-type structure with no

gold-related features (see Figure S-1). As discussed previously, the majority of the gold is proposed to be present as highly dispersed gold particles in direct contact with the ceria support rather than particles observable with TEM or XRD.[1,2] The presence of gold was confirmed by X-ray photoelectron spectroscopy (XPS, see Section 1.3).

1.2 Gas Sensing

For sensor preparation, the ceria-based samples (~50 mg) were ultrasonically dispersed in deionized water and then dropped onto the surface of an Al_2O_3-transducer substrate with interdigitated Pt-electrodes (electrode distance ~150 µm) to measure the sheet resistance. On the other side of the substrate was a meander Pt-heater to heat the sensing material. The sensor was annealed at 85°C. The sample resistance was measured using a Keithley 175A Autoranging Multimeter. The temperature of the Pt-heater was calibrated prior to experiments. For gas sensing experiments, the following gases (Westfalen AG) were used: oxygen 5.0 (≤ 0.2 ppm CO_2, ≤ 0.2 ppm C_nH_m, ≤ 3 ppm H_2O, ≤ 10 ppm N_2 + Ar), nitrogen 5.0 (≤ 3 ppm O_2, ≤ 1 ppm C_nH_m, ≤ 5 ppm H_2O), and 1000 ppm ethanol in nitrogen 5.0. The used carrier gas was synthetic air or nitrogen cycled with 250 ppm ethanol in synthetic air or nitrogen fed at 80 mL/min.

The gold containing ceria gas sensors showed a strongly improved recovery behavior after exposure to EtOH/air compared to bare ceria gas sensors. Defining the recovery as the ratio of resistance as measured in air before and 30 min after exposure to EtOH/air, the 0.5 wt% Au/CeO_2 (CeO_2) gas sensor yielded recoveries of 0.86 (0.14) and 0.90 (0.30) at 200°C and 300°C, respectively.

1.3 Spectroscopic Characterization

X-Ray Photoelectron Spectroscopy. X-ray photoelectron spectroscopy (XPS) was performed on a modified LHS/SPECS EA200 system using a Mg Kα source (1253.6 eV, 168 W). XP spectra were recorded under UHV conditions. Calibration was done based on the Au 4f signal of gold foil at 84.0 eV and the Cu 2p signal of a copper plate at 932.7 eV.[3] Sample charging was accounted for by setting the Ce 3d u‴ signal to 916.7 eV.[4] This corresponds to a C 1s position of 284.7 eV, in agreement with literature values for ubiquitous carbon.[4]

As shown in Table S-1, XPS analysis demonstrates the presence of gold in 0.5 wt% Au/CeO_2 and 1 wt% Au/CeO_2. Au 4f detailed spectra reveal that gold is present as Au and Au^+. The fraction of Au^+ was determined to be ~42%. Based on C 1s detailed spectra, the presence of the carbon signal is mainly attributed to ubiquitous carbon as well as some carbonate (16-17%).

Raman Spectroscopy. Raman spectra were collected in a 180° backscattering geometry using a 20× objective (Olympus SLMPLN20x, WD: 25 mm, NA: 0.25). For excitation, we employed an Ar^+ laser (Melles Griot) operated at 514.5 nm. The applied laser power was 1.5 mW as measured with a power meter at the sample location (Ophir). As previously confirmed, at that power level and wavelength, there was no damage on the sample even after several hours of laser irradiation. The backscattered light was dispersed using a HoloSpec *f*/1.8i Raman spectrometer (Kaiser Optical Systems) with an axial transmission grating and sent to a Peltier-cooled charge-coupled device (CCD) for detection. The resolution of the spectrometer is 5 cm^{-1}; however, the wavelength stability was better than 0.5 cm^{-1} as confirmed in a large number of previous Raman spectroscopic studies on ceria-based and other oxide materials, see e.g. Refs. [1, 4-7]. Based on these studies the error bars are given as ±0.25 cm^{-1}.

Raman spectra were collected continuously with an accumulation time of 1200 s, including the application of a cosmic ray filter and subtraction of the dark spectrum (laser off). The

poly(tetrafluoroethylene) (PTFE) cell used for all Raman experiments made no observable contribution to the Raman signal. Besides, gas-phase signals or signals of adsorbates on the Al_2O_3 transducer substrate or the PTFE walls were not observed. Raman spectra were absorption corrected using the G(∞) factor as described in detail elsewhere.[8] To determine the positions of the F_{2g} bands a peak fitting analysis was applied using Lorentzian functions.

Figure S-2 shows the Raman spectrum of the 0.5 wt% Au/CeO_2 gas sensor at 400°C in air using 514.5 nm laser excitation; the spectrum is characterized by features at 237 cm^{-1}, at around 400 cm^{-1} (shoulder), at 454 cm^{-1}, at around 560 cm^{-1}, as well as at 1160 cm^{-1}. The strong band at 454 cm^{-1} is due to the F_{2g} mode; the minor band at 1160 cm^{-1} is a second-order Raman mode (2LO). The features at 237 and 400 cm^{-1} originate from the longitudinal and transversal stretching mode of surface oxygen against cerium (Ce-O), respectively, in agreement with DFT+U calculations.[9,1] The Raman feature at around 560 cm^{-1} consists of (at least) two contributions. Based on prior DFT+U results the band in the region 560 cm^{-1} can be assigned to Ce^{3+} in the vicinity of an oxygen vacancy, whereas a band at 540 cm^{-1} points to Ce^{3+} further away from an oxygen vacancy.[9,1] Details of the Raman band assignment have been described previously.[6,9,1]

Operando **Spectroscopy.** A scheme of the experimental setup used for the *operando* experiments is shown in Figure S-3. Raman spectra were recorded in a homebuilt PTFE cell as described above. Products were analyzed by FTIR spectroscopy (Bruker Vertex 70 FTIR spectrometer, pyroelectric DLaTGS (deuterated L-alanine doped triglycene sulfate) detector) in a small-volume (25 mL) gas cell (Axiom, LFT) heated to 125°C to avoid condensation. IR spectra were measured continuously with a resolution of 4 cm^{-1} and a measurement period of 300 scans (~250 s) using the carrier gas as a reference. Table S-2 summarizes the assignment of the IR gas-phase bands. To correlate the IR and gas-sensing measurements, the IR bands

were baseline corrected and their intensities were plotted against time. Any ethanol contribution was subtracted.

Figure S-4 shows *operando* Raman spectra of the ethanol gas sensing by 0.5 wt% Au/CeO_2 recorded at 514.5 nm excitation, corresponding to the data shown in Figure 2. The F_{2g} band is cut off to give an enlarged view of the spectral features up to 1700 cm^{-1}; the F_{2g} band positions correspond to those given in Figure 2. As discussed above, the features at 237 and 400 cm^{-1} originate from surface stretching modes of surface oxygen against cerium (Ce-O). In EtOH/N_2 flow, these features show a decrease in intensity, particularly at 325°C; however, quantification is difficult due to the low-wavenumber cut-off and the overlap with the strong F_{2g} band.

In Figure S-5 *operando* Raman spectra (514.5 nm) of a CeO_2 gas sensor in various gas environments at 190°C are depicted; the overall spectral behavior of the high-wavenumber region is somewhat similar to that of In_2O_3 gas sensors reported previously,[7] but there are distinct differences as discussed below. At 190°C in nitrogen, the Raman spectrum of CeO_2 is characterized by a broad feature at around 3643 cm^{-1}, which has previously been attributed to bridged hydroxyl species.[10,11] Upon exposure to EtOH/N_2, new bands appear at 2848, 2877 (shoulder), 2932, and 2969 cm^{-1}, whereas the hydroxyl-related feature is not observed anymore. The Raman band at 2848 cm^{-1} and part of the Raman band at 2932 cm^{-1} are attributed to a formate species, in agreement with the literature on CeO_2,[12] whereas the shoulder at 2877 cm^{-1} may indicate the presence of second type of formate species.[7] Please note that the latter behavior contrasts that on In_2O_3 gas sensors, where only one type of formate species has been observed.[7] Raman bands at 2938 and 937 cm^{-1} have previously been assigned to acetate in the context of In_2O_3 gas sensors.[7] Here, besides the 2932-cm^{-1} band, a weak feature is observed at around 950 cm^{-1} (not shown); thus the presence of acetate species is proposed. The weak band at 2969 cm^{-1} is indicative of adsorbed ethanol.[7] Figure S-5 shows that switching to air flow leads to a strong decrease of the adsorbate features, whereas the hydroxyl-related

band reappears. The Raman spectrum in EtOH/air flow resembles the spectrum in EtOH/N_2 discussed above but indicates a larger faction of formate species.

1.4 Raman Probe Depth

The sampling depth of Raman experiments was examined in previous studies on 0.5 wt% Au/CeO_2 prepared according to the same synthesis protocol as in the present study. Please note that the results of the characterization of those samples resemble those of the sample studied here. As described in detail elsewhere,[5] using isotope experiments, we were able to show that exposure of Au/CeO_2 to CO/$H_2{}^{18}O$/Ar leads to a more intense ^{18}O F_{2g} phonon band. However, after cooling in an argon flow, an F_{2g} band at the original ^{16}O position was observed. Thus Raman spectroscopy probes only the subsurface layers of the ceria particle, where ^{18}O agglomerates during exposure to CO/$H_2{}^{18}O$/Ar, while a fraction of oxygen in the ceria particle remains ^{16}O. As a consequence, after exposure to CO/$H_2{}^{18}O$/Ar, equilibration of ^{18}O within the whole particle leads to a dilution of ^{18}O in the subsurface region and a dominant ^{16}O F_{2g} phonon is measured by Raman spectroscopy. Based on these observations on the F_{2g} phonon, we deduce the Raman probe depth to be confined to the *subsurface* region of the ceria particle rather than the whole ceria particle or the *bulk*.

Supplementary Figures and Tables

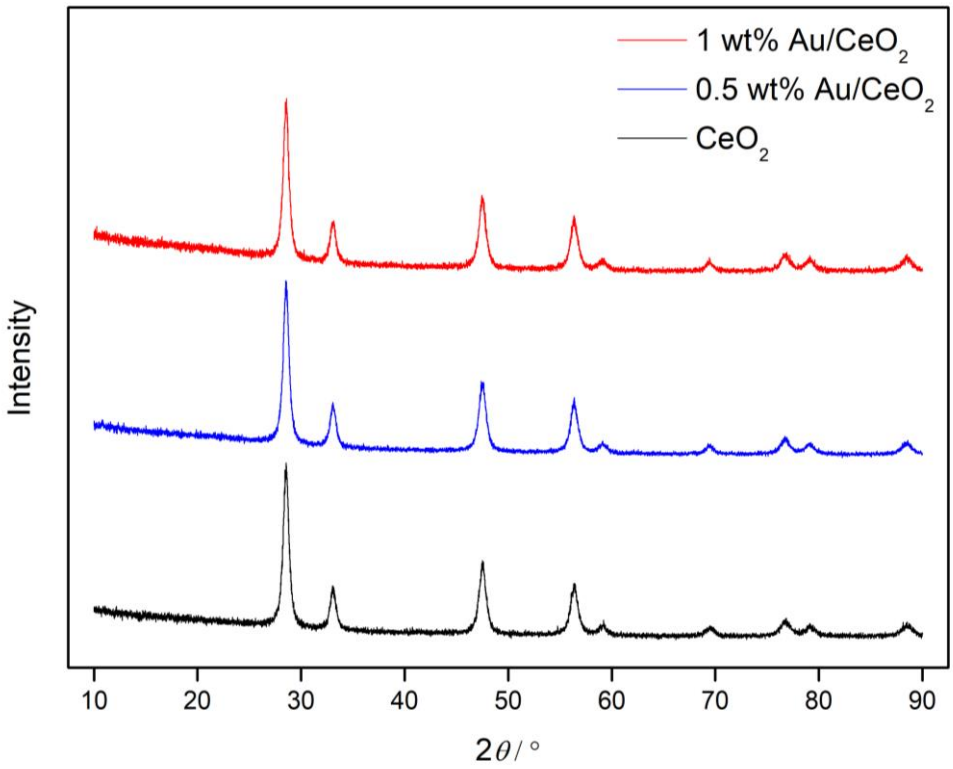

Figure S-1. X-ray diffraction patterns of the prepared sensor materials CeO_2, 0.5 wt% Au/CeO_2, and 1 wt% Au/CeO_2. Traces are offset for clarity.

Table S-1. Surface composition of the Au/CeO_2 samples based on the XPS analysis.

sample	Au / at%	Ce / at%	O / at%	C / at%
0.5 wt% Au/CeO_2	0.5	25.8	59.5	14.2
1 wt% Au/CeO_2	1.2	23.8	58.9	16.1

Table S-2. Assignment of the IR gas-phase bands used for the correlation in Figure 2.

wavenumber (cm^{-1})	gas
2903	EtOH
2361	CO_2
2733	H_3C-CH=O

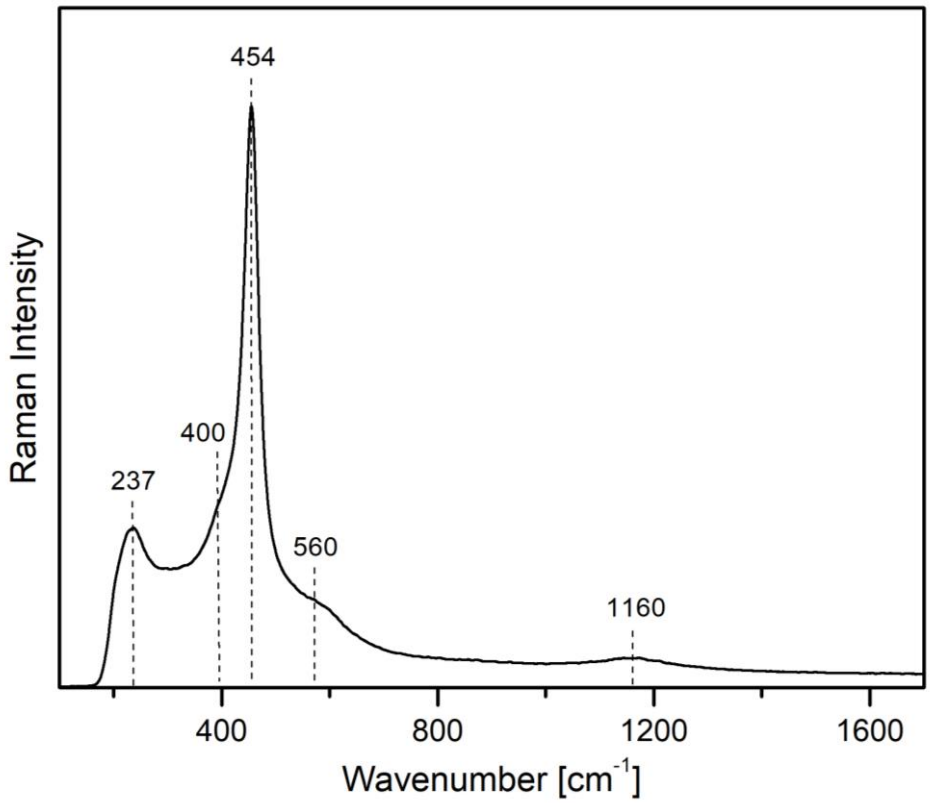

Figure S-2. Raman spectrum of the 0.5 wt% Au/CeO_2 gas sensor at 400°C in air at 514.5 nm.

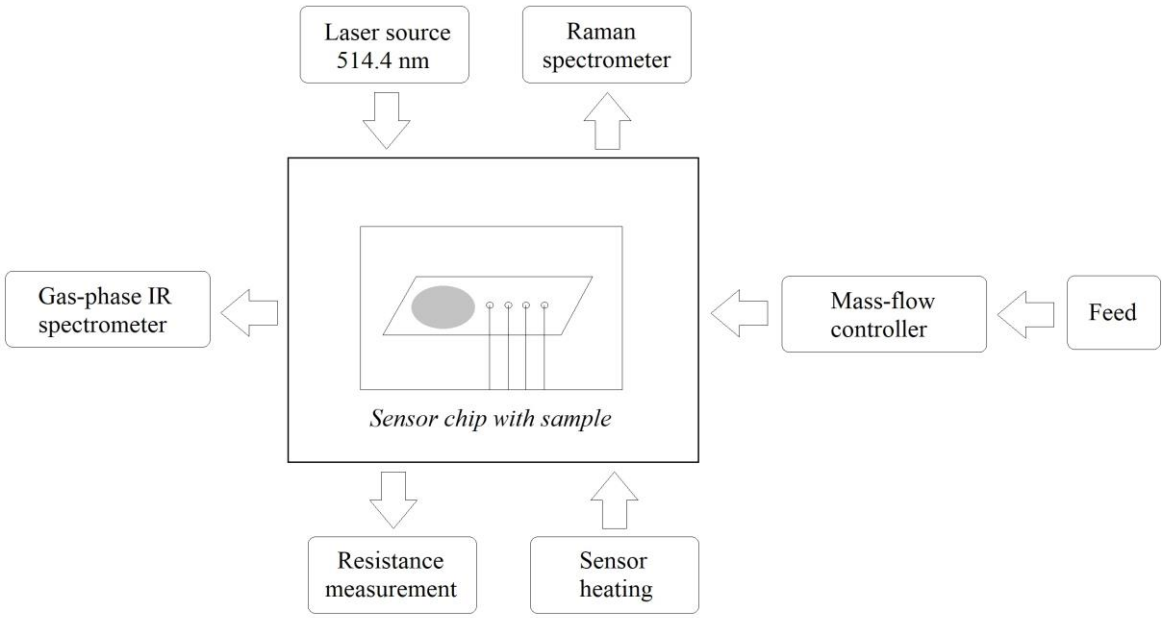

Figure S-3. Scheme of the setup used for the *operando* experiments.

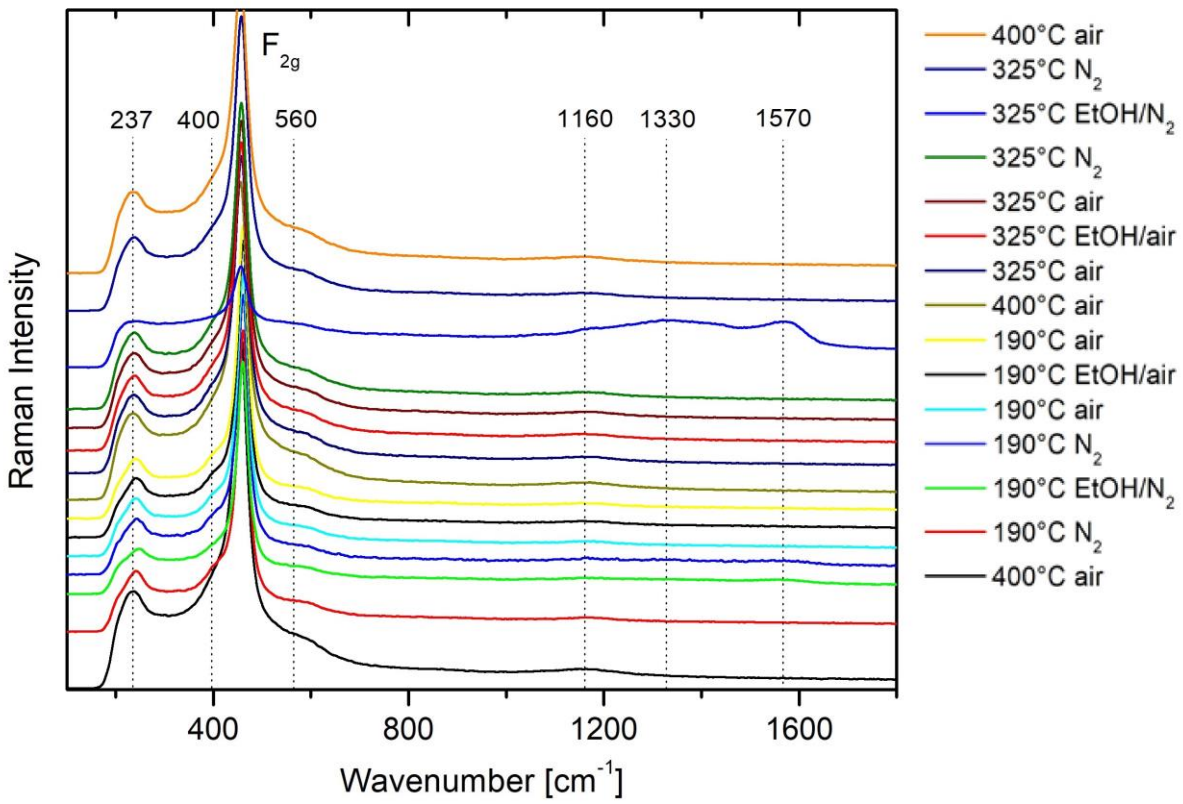

Figure S-4. *Operando* Raman spectra of the ethanol gas sensing by 0.5 wt% Au/CeO_2 recorded at 514.5 nm excitation. The F_{2g} band is cut off; the F_{2g} band positions correspond to those given in Figure 2. Spectra are offset for clarity.

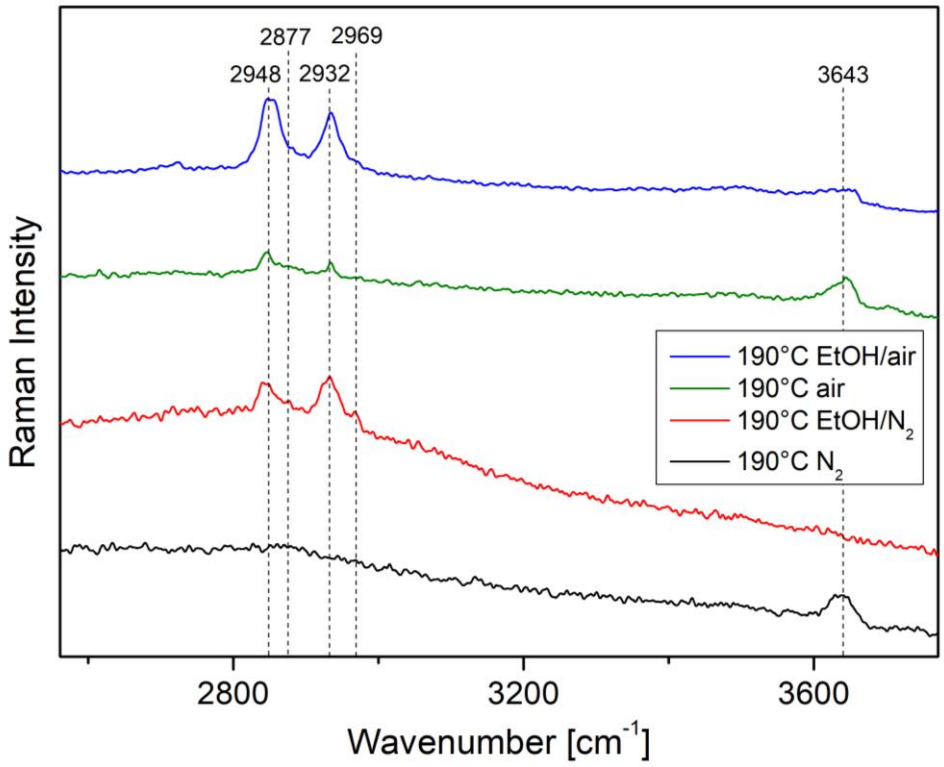

Figure S-5. *Operando* Raman spectra of the ethanol gas sensing by CeO_2 recorded at 514.5 nm excitation. Spectra are offset for clarity.

References

1 Schilling, C.; Hess, C. Real-Time Observation of the Defect Dynamics in Working Au/CeO_2 Catalysts by Combined Operando Raman/UV-Vis Spectroscopy. *J. Phys. Chem. C* **2018**, *122*, 2909-2917.

2 Fu, Q.; Saltsburg, H.; Flytzani-Stephanopoulos, M. Active Nonmetallic Au and Pt Species on Ceria-Based Water-Gas Shift Catalysts. *Science* **2003**, *301*, 935-938.

3 Moulder, J. F.; Stickle, W. F.; Sobol, P. E.; Bomben, K. D. *Handbook of X-ray photoelectron spectroscopy*; Perkin Elmer, Eden Prairie, MN; 1992; Vol. 40.

4 Nottbohm, C. T.; Hess, C. Investigation of Ceria by Combined Raman, UV-vis and X-Ray Photoelectron Spectroscopy. *Catal. Commun.* **2012**, *22*, 39-42.

5 Schilling, C.; Hess, C. Elucidating the Role of Support Oxygen in the Water–Gas Shift Reaction over Ceria-Supported Gold Catalysts Using Operando Spectroscopy. *ACS Catal.* **2019**, *9*, 1159-1171.

6 Filtschew, A.; Hofmann, K.; Hess, C. Ceria and Its Defect Structure: New Insights from a Combined Spectroscopic Approach. *J. Phys. Chem. C* **2016**, *120*, 6694-6703.

7 Sänze, S.; Hess, C. Ethanol Gas Sensing by Indium Oxide: An Operando Spectroscopic Raman-FTIR Study. *J. Phys. Chem. C* **2014**, *118*, 25603-25613.

8 Filtschew, A.; Hess, C. Interpretation of Raman Spectra of Oxide Materials: The Relevance of Absorption Effects. *J. Phys. Chem. C* **2018***, 121*, 19280-19288.

9 Schilling, C.; Hess, C.; Ganduglia-Pirovano, M.V. Raman Spectra of Polycrystalline CeO_2: A Density Functional Theory Study. *J. Phys. Chem. C* **2017**, *121*, 20834-20849.

10 Badri, A.; Binet, C.; Lavalley, J. C. An FTIR Study of Surface Ceria Hydroxy Groups During a Redox Process with H_2. *J. Chem. Soc., Faraday Trans.* **1996**, *92,* 4669-4673.

11 Filtschew, A.; Hess, C. Unravelling the Mechanism of NO and NO_2 Storage in Ceria: The Role of Defects and Ce-O Surface Sites*. Appl. Catal. B* **2018**, *237*, 1066-1081.

12 Swanson, M.; Pushkarev, V. V.; Kovalchuk, V. I.; d'Itri, J. L. The Dynamic Surface Chemistry During the Interaction of CO with Ceria Captured by Raman Spectroscopy. *Catal. Lett.* **2007**, *116*, 41-45.